Korean J. Chem. Eng., 37(10), 1751-1760 (2020)
DOI: 10.1007/s11814-020-0568-4

pISSN: 0256-1115
eISSN: 1975-7220

Bio-inspired antifouling Cellulose nanofiber multifunctional filtration membrane for highly efficient emulsion separation and application in water purification

Xiangying Yin*,, Yi He*,**,†, Yuqi Wang*,**, Hao Yu*,**, Jingyu Chen***,†, and Yixuan Gao*,****

*State Key Laboratory of Oil & Gas Reservoir Geology and Exploitation, Southwest Petroleum University, Chengdu, Sichuan 610500, P. R. China
**College of Chemistry and Chemical Engineering, Southwest Petroleum University, Chengdu, Sichuan 610500, P. R. China
***Deakin University, Institute for Frontier Materials, VIC 3220, Australia
(*Received 19 June 2019 • Revised 25 March 2020 • Accepted 5 May 2020*)

Abstract−Membrane fouling is usually a troublesome issue in oily water treatment, especially containing complex crude oil emulsions. Although most of the reported membranes are in a position to repel models oils, it's still a big challenge of repelling crude oil. Besides, the fabrication processes of those membranes are too complicated, high-cost and environmentally unfriendly. Hence, in this work, a facile and green method was designed to fabricate a Cellulose nanofiber (CNF) polyelectrolyte filtration membrane with excellent underwater superoleophobic characteristic and outstanding antifouling performance. The membrane not only can separate oil/water emulsions with a high separation efficiency (>99%) and water flux (>11,000 L m^{-2} h^{-1}), but also remove positively charged dyes with good permeation fluxes (>10,000 L m^{-2} h^{-1}) and rejection radio (>98%). Herein, it can be anticipated that this method has excellent potential for designing and preparing the specific membranes for multifunctional applications in water treatment.

Keywords: Cellulose Nanofiber, Membrane, Emulsion Separation, Antifouling

INTRODUCTION

In terms of the increasingly severe wastewater problem, such as frequent oil recovery activities and industrial discharge of oily wastewater, oily wastewater treatment issue has always been a research focus [1-3]. Thus, it is urgent to develop effective technologies of oil/water separation from both economic and environmental perspectives. Current methods of water purification contain chemical coagulation, solvent extraction, ion exchange, absorption, membrane separation and so on [4-7]. In contrast, in view of its high efficiency, a simple operation process and no chemical additives, membrane-based filtration technologies have been developed as promising routes for water purification [8,9]. Among them, polymer-based materials, including polyacrylonitrile (PAN), polysulfone (PS), polypropylene (PP), poly(vinylidene fluoride) (PVDF), have become the majority of filtration membranes due to the low-cost and easily-fabricated [10-14]. However, as far as oil/water separation is concerned, traditional polymer-based membranes often suffer from undesired serious fouling owing to oil adsorbing and settling onto the surface, which leads to irreversible decline of separation performance and lifespan efficiency [15]. For instance, the problem of membrane fouling is usually troublesome in the process of emulsion treatment [16-18]. Thus, further large-scale practical applications of filtration membranes are restricted.

In fact, surface hydrated layer, which protects the surface from contacting, endows the filtration membrane with antifouling performance [19-21]. The stronger the extent of hydration, the superior is the antifouling function [22,23]. Polyelectrolyte is a representative material that usually has strong hydration ability [24]. Due to abundant hydrophilic groups on polyelectrolytes, such as hydroxy, carboxyl, amino, polyionized group, on polyelectrolytes can develop a powerful hydration film in water [25,26]. Recently, according to Brown and Bhushan [27], a robust antifouling superoleophobic/superhydrophilic coating could be formed with the polyelectrolyte-fluorosurfactant complex by layer-by-layer method. Besides, a superhydrophilic/underwater superoleophobic polyacrylonitrile with alkaline condition was reported by Zhang et al. [28], and the composite separation membrane showed an ultralow oil-adhesion behavior. Furthermore, He et al. [29] covered polyelectrolyte coating onto the steel mesh with the method of surface-initiated atom transfer radical polymerization (SI-ATRP). After modification, the steel mesh had excellent self-cleaning property in a wet state. Although those membranes with antifouling property can be used for oil/water mixtures separation, the fabrication processes are too complicated and materials are high-cost and environmentally unfriendly [30,31]. As a result, the demand for developing convenient methods with green materials to fabricate antifouling membranes has never stopped.

The Cellulose nanofiber (CNF) is regarded as the next generation renewable polyelectrolyte for the production of high performance composites due to biocompatibility, biodegradability, large specific surface, excellent adsorption capacity and low-cost [32-38]. Alternatively, the huge amount of surface hydroxyl makes it sensitive to

Electronic supplementary material The online version of this article (https://doi.org/10.1007/s11814-020-0568-4) contains supplementary material, which is available to authorized users.

†To whom correspondence should be addressed.
E-mail: chemheyi@swpu.edu.cn, jingyu.chen@deakin.edu.au

moisture absorption on account of the intra- and inter-molecules hydrogen bonds in water, which is equipped with extraordinary hydrophilicity [39-42]. Thus, CNF has attracted attention in the construction of antifouling surface owing to its strong hydration and excellent performance to repelling oils [43]. It implies that the CNF opens a promising avenue in advanced separation membrane. As far as we know, scant studies have focused on combining CNF on polymer filtration substrates to obtain an excellent antifouling separation membrane.

Under oxidizing conditions, dopamine is capable of self-polymerizing in alkaline condition, forming a tightly adhesive polydopamine (PDA) layer on the substrate [44]. Although the molecular mechanism of PDA formation is quite complicated, it is believed to originate from strong covalent and non-covalent bonds between substrates and catecholic derivatives of either small molecules or macromolecules [45]. At the same time, the deposition of PDA can be a flat to conduct secondary reaction, because many functional groups (planar indole units, aimo group, carboxylic acid group, catechol or quinone functions and indolic/catecholic π-systems) are integrated into PDA [46-48]. In this work, we employed dopamine as a binder and put forward a facile method to fabricate a novel CNF@PDA filtration membrane with hierarchical architecture and underwater superoleophobicity (Scheme 1). The resulting CNF@PDA membrane not only showed excellent separation efficiency for various oil/water emulsions but also demonstrated excellent anti-oil-fouling performance. All in all, the excellent performance and convenient fabrication method of the CNF@PDA membrane hold a great prospect in real-world scalable wastewater treatment.

METHODS AND MATERIALS

1. Materials

Tris (hydroxymethyl) aminomethane hydrochloridel (Tris-HCl) (≥99%) and dopamine hydrochloride (DA) (98%) were provided by Aladdin Biochemical Technology Co, Ltd. (Shanghai, China). Cellulose acetate membranes (average pore size: 0.22 μm), sodium dodecyl sulfate (SDS) (99%) were provided by Kelong Chemical Co, Ltd. (Chengdu, China). All reagents were all analytical grades. Cellulose nanofiber (20-50 nm in diameter, the length >1 μm) were prepared by TEMPO (2, 2, 6, 6-tetramethylpiperidine-1-oxyl radical)-mediated oxidation, which were customized by Zhongshan NFC Bio-materials Co., Ltd. Low viscidity crude oil was used for oil/water emulsion separation, and UOCA and high viscidity crude oil was used for adhesive force measurement. Both of them were obtained from local oilfield in Daqing.

2. Preparation of PDA-coated Cellulose Acetate Membrane

First, as a substrate, Cellulose acetate membrane was cut into 2.5×2.5 cm^2 square pieces. 0.04 g DA was added into 20 ml Tris-HCl solution (pH 8.5) and mixed the solution. Next, the substrate was put into the solution and the solution was stirred at 70 °C for 12 h to obtain a rough PDA surface layer. Then the membrane was rinsed with deionized (DI) water overnight. The PDA-coated membrane was dried by nitrogen gas or in a vacuum oven at 25 °C for 12 h before using.

3. Preparation of CNF-PDA-coated Cellulose Acetate Membrane (CNF@PDA)

A certain amount of cellulose nanofibers (0.5 mg ml^{-1}) and Tris-HCl (1.6 mg ml^{-1}) were dispersed in DI water under ultrasonic wave and stirring to obtain a stable suspension (pH 8.5). Then samples of PDA-coated membrane were immersed in the suspension, and the solution was stirred at 50 °C for 24 h. Next the modified membrane was washed with DI water adequately. In the end, the CNF@PDA was dried with nitrogen gas or in a vacuum oven at 25 °C for 12 h before using.

4. Preparation of Pure CNF Membrane

A series of cellulose nanofibers were dispersed in DI water under

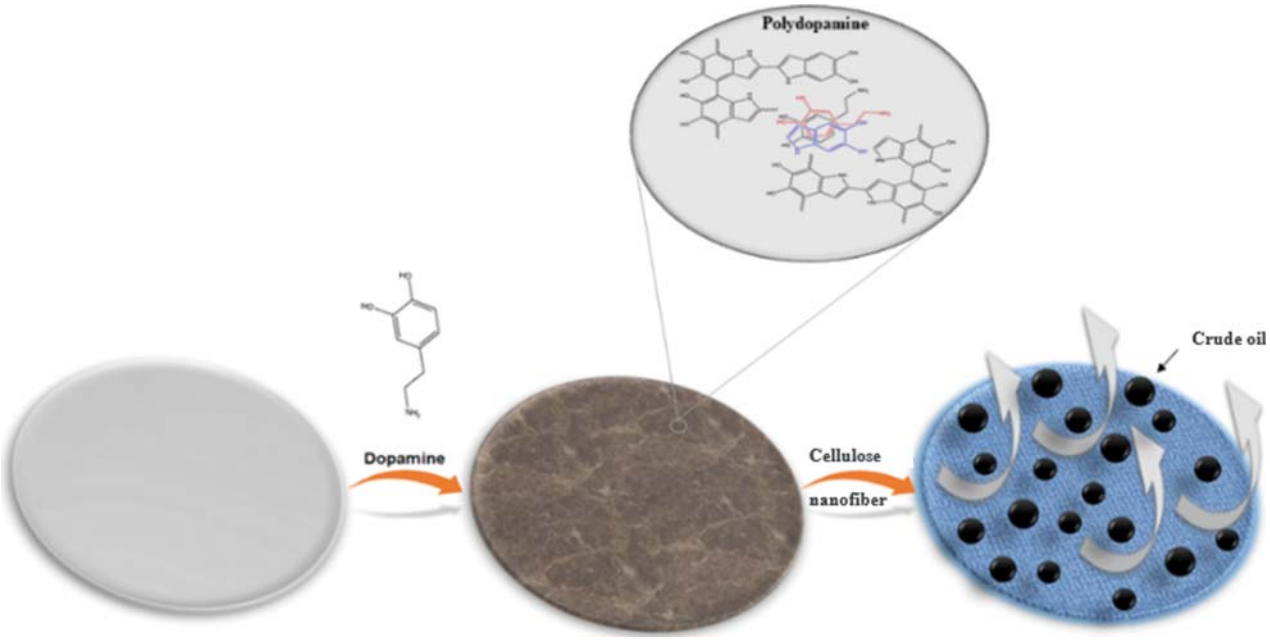

Scheme 1. Schematic illustration for the reaction process of modified membranes.

ultrasonic wave and stirred to acquire a stable CNF suspension. Then the pure CNF membranes were prepared by vacuum-assisted filtration of CNF suspension on Cellulose acetate membranes. The pure CNF membrane was dried by nitrogen gas or in a vacuum oven at 25 °C for 12 h before using.

5. Preparation of Oil-in-water Emulsions

The surfactant-free (SF) oil-in-water (O/W) emulsions were mixed by oils (diesel, cydohexane, toluene, low viscidity crude oil) and water (volume ratio=1 : 99) and stirred at 1,000 rpm for 30 minutes. The SF emulsions remained stable for about 24 h without obvious demulsification. The surfactant-stabilized (SS) oil-in-water emulsions were prepared with similar method, except dissolving SDS of 100 mg L^{-1} in the water at first and the SS emulsions were also maintained stable more than 24 h.

6. Characterization

Scanning electron microscopy (SEM) and Energy dispersive spectroscopy (EDS) (JSM-7500F, JEOL) were employed to investigate the morphology and compositions of the modified membranes. The changes in chemical functional groups were analyzed by Fourier transform infrared spectroscopy (FT-IR) (Thermo Fisher Nicolet iS10). The pore size of the above membranes was examined by a bubble pressure membrane pore size analyzer (3H-2000PB, Bei Shi De Technology (Beijing) Co., Ltd., China). Besides, Zeta potential of modified membranes surface was determined by using the zeta potential analyzer (Zata PALS 190 Plus, Brookhaven, United States). Water contact angle (WCA) and underwater oil contact angle (UOCA) were characterized by Contact angle goniometer (Beijing Hake, XED-SPJ) at ambient temperature with a 4 μL water or oil droplet, respectively. The oil concentration in emulsions and filtrates was analyzed by Total organic carbon (TOC) (Shimadzu TOC-VCPH analyzer). The as-prepared emulsions and filtrate samples were also studied with an optical microscope (Nikon Digital Sight DS-F11, Japan). In addition, concentration changes of dye solution were measured by UV-spectrophotometer (Shimadzu, UV-1800).

7. Separation Performance

The performance of oil/water separation was studied by using the dead-end model filtration device. The as-prepared membranes were fixed onto a circular sand filter with an effective surface area of 1.767 cm^2. DI water permeation and emulsion separation test were conducted under 0.09 MPa with assistance of the pump. Before testing, the as-prepared membrane was compacted with DI water until a stable flux was obtained. First, water permeability was measured. Then the emulsion was actuated to permeate through the membrane (the process is shown in Movie S1, Movie S2 and Movie S3, Supporting Information). The permeation flux (L m^{-2} h^{-1}) was calculated using Eq. (1):

$$J = \frac{v}{A_{ef}t} \tag{1}$$

where J is the permeation flux (L m^{-2} h^{-1}), v is the permeation volume of filtrate that passed through the membrane in a predetermined time t, and A_{ef} is the effective filtration area.

The separation efficiency (S) was calculated using Eq. (2):

$$S(\%) = \left(1 - \frac{C_p}{C_f}\right) \times 100\% \tag{2}$$

where C_p and C_f (mg L^{-1}) correspond to oil concentration in filtrates and feed solution.

The performance of modified membrane dye removal was evaluated with dye solutions (Methylene blue (MB) and Gentian violet (GV)) using a UV spectrophotometer. The rejection ratio (R) was calculated with Eq. (3):

$$R(\%) = \left(1 - \frac{C_p}{C_f}\right) \times 100\% \tag{3}$$

where C_p and C_f (mg L^{-1}) correspond to dye concentration of filtrate and feed solution, respectively.

The flux recovery ratio (FRR) was calculated with Eq. (4):

$$FRR(\%) = \left(\frac{J_{w2}}{J_{w1}}\right) \times 100\% \tag{4}$$

where J_{w1} and J_{w2} (L m^{-2} h^{-1}) correspond to pure water flux before and after filtering emulsions, respectively.

RESULTS AND DISCUSSION

1. Preparation and Characterization of Modified Composite Membrane

Since the pioneering work on CNF, CNF has been an ideal material from which to base a new biopolymer composite membrane industry. In terms of a facile method (Fig. 1(a)), CNF@PDA membranes were effectively prepared [49-51]. And the FT-IR spectrum was used to verify the surface functional groups of modified membranes. As shown in Fig. 1(b), two curves are ascribed to only PDA-coated (black line) and CNF@PDA membrane (red line). A characteristic carbonyl (C=O) stretching band around 1,642 cm^{-1} and a characteristic hydroxyl (O-H) stretching band at 3,460 cm^{-1} can be observed [52]. Absorption peaks as mentioned above in FT-IR are assignable to characteristic functional groups of cellulose acetate substrate. The present absorption peaks at 1,282 cm^{-1}, 1,470 cm^{-1} and 1,602 cm^{-1} were assigned to the -C-OH, N-H and C=C, respectively, and these peaks were derived from PDA. Furthermore, after modified CNF, a noticeable new sharp peak in protonated CNF at 2,900 cm^{-1} is C-H stretching band, and 1,749 cm^{-1} is attributed to C=O of the carboxylic acid which confirmed the oxidation of C-6 of cellulose after TEMPO oxidation [53]. As shown in Fig. S1 (Supporting Information), the correlative characteristic peak of CNF@PDA membrane is the same as pure CNF membrane, which demonstrates the CNF was successfully modified on the membrane surface.

The surface morphology of the membranes was characterized by SEM. From the results of Fig. 1(c), (d), all membranes exhibited a typical porous surface structure. PDA-coated membrane exhibited a rough surface structure. As far as the CNF@PDA is concerned, the CNF was expected to decrease the surface roughness and pore size. In addition, the surface area could be enlarged, simultaneously. As a result, the morphology of CNF@PDA membrane surface was smoother, and the pore size was much smaller than only PDA-coated membrane, due to the connection between CNF and PDA. To further verify our hypothesis, the average pore size and pore size distribution of various modified membranes were measured. For the substrate, the average pore size was 220 nm, which

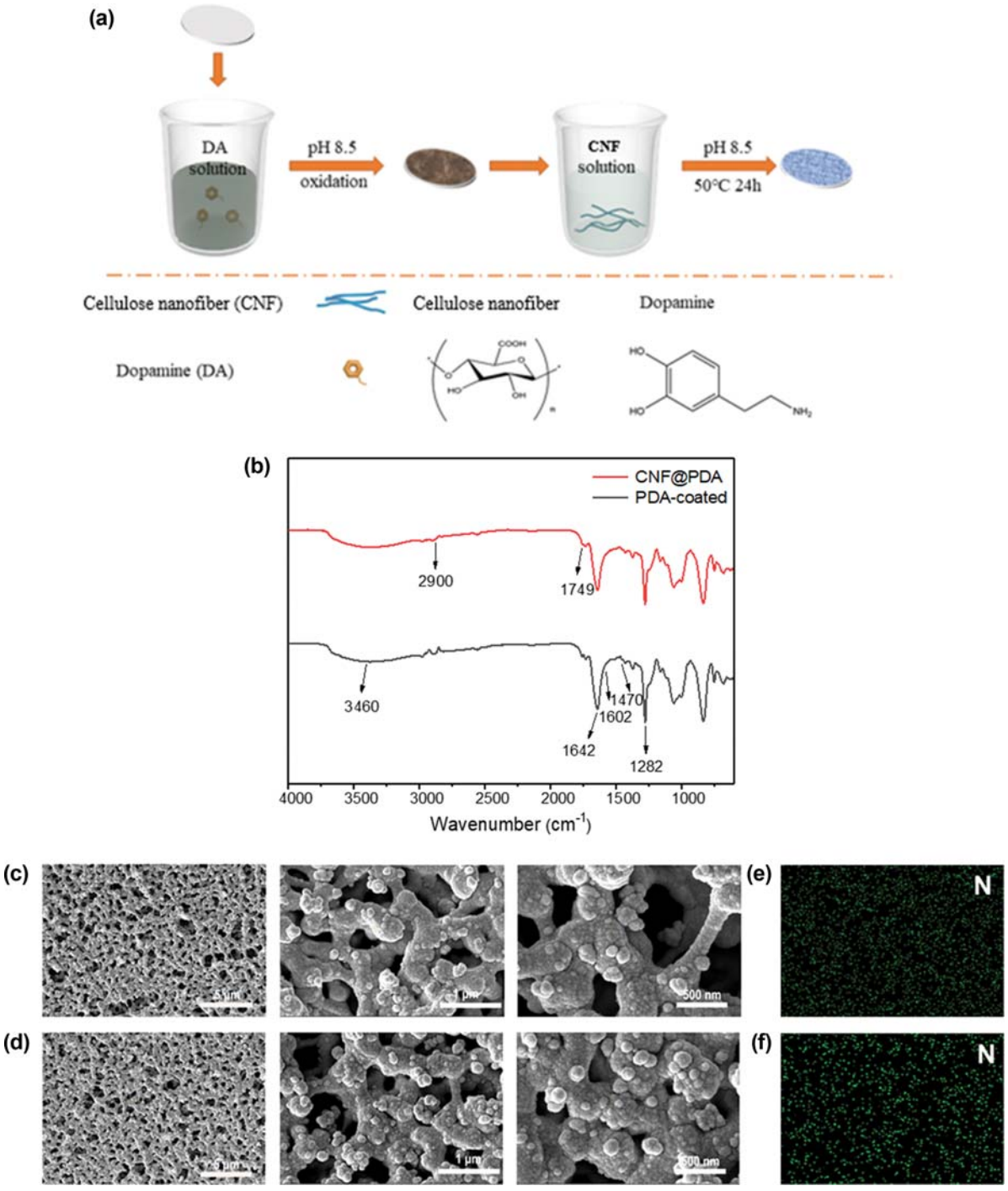

Fig. 1. (a) Schematic diagram of CNF and DA modified Cellulose acetate membrane. (b) FT-IR of PDA-coated and CNF@PDA membranes. (c) and (d) SEM of PDA-coated and CNF@PDA membranes, respectively. (e) and (f) nitrogen EDS mapping image of PDA-coated and CNF@PDA membranes, respectively.

Table 1. The average pore size PDA-coated and CNF@PDA membranes

Type of membrane	Average pore size (nm)
PDA-coated	190.2
CNF@PDA	167.7

Table 2. Surface element characterization of membranes involved in this study

Samples	Atomic percentage (at%)		
	C	N	O
PDA-coated	51.86	10.54	37.60
CNF@PDA	53.42	5.39	41.19

was supported by Kelong Chemical Co, Ltd. (Chengdu, China). As shown in Table 1, after modification, the pore size of CNF@PDA was reduced to 167.7 nm and uniformly the pore size distribution (Fig. S2, supporting Information). This result agreed with the SEM images which were described previously. The EDS analysis (Table 2) implied that the CNF was successfully modified since the con-

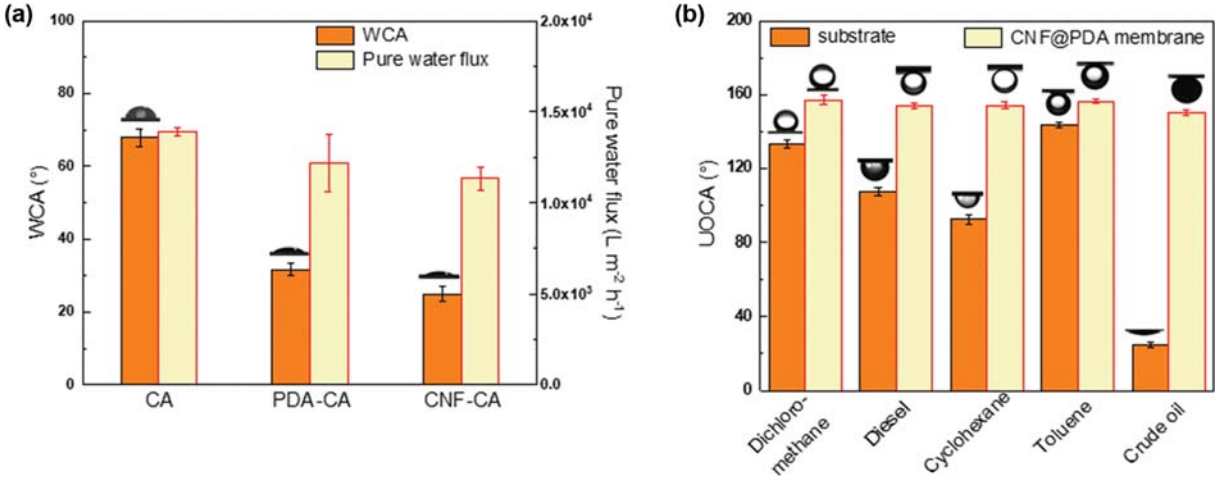

Fig. 2. (a) WCA and pure water flux of substrate, PDA-coated, CNF@PDA membranes, respectively. (b) UOCA for various oils of substrate, CNF@PDA membranes, respectively.

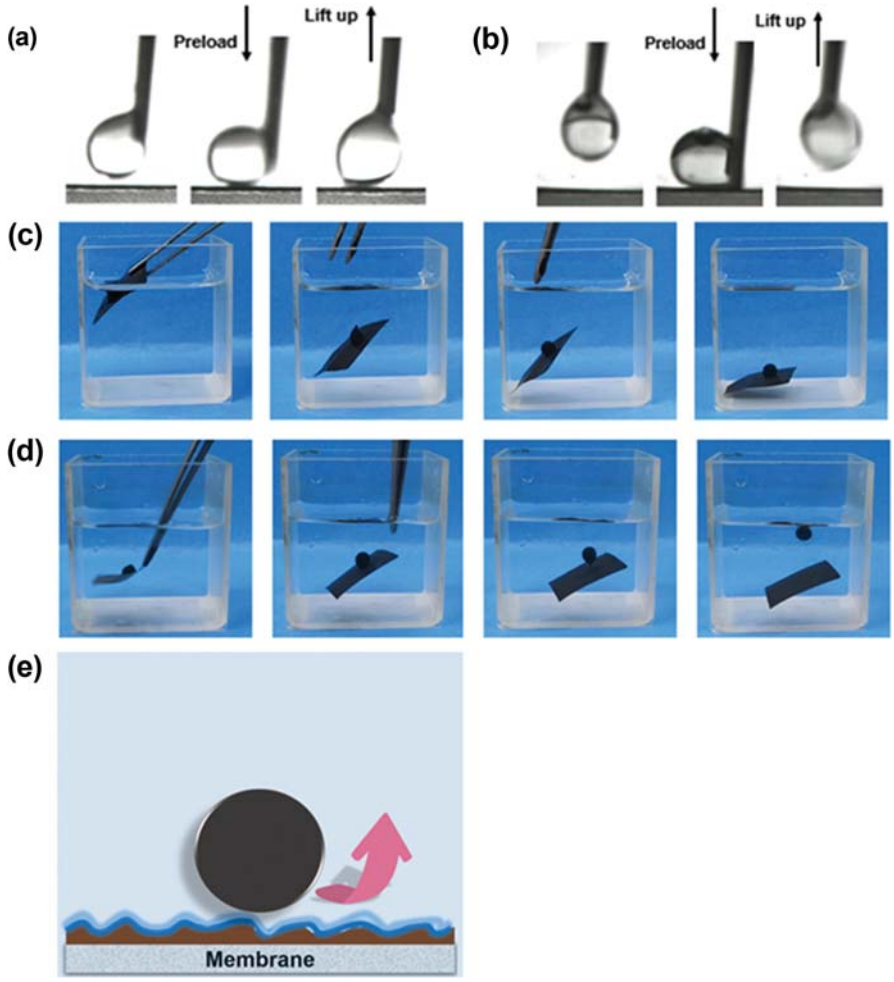

Fig. 3. (a), (b) Dynamic underwater oil-adhesion of PDA-coated and CNF@PDA membranes, respectively. (c), (d) Anti-crude-oil adhesion of PDA-coated and CNF@PDA membranes, respectively. (e) The mechanism of anti-oil-adhesion performance.

tent of nitrogen element of CNF@PDA decreased and the oxygen increased obviously. In addition, element analysis of PDA-coated membrane and CNF@PDA membrane was obtained by EDS mapping image. As shown in Fig. 1(e), (f), it is clear that after CNF modified the PDA-coated membrane, the nitrogen content was reduced. Moreover, corresponding EDS mapping images also showed the distribution of elements, proving the uniform distribution of CNF.

2. Surface Wetting Behavior and Antifouling Performance

It was well-known that the surface wetting behavior is controlled by the chemical constitution and morphology of the membrane surface. Due to the inherent hydrophilicity and nanoscale dimensions of CNF and PDA (Fig. 1(c), (d)), the prepared membranes exhibited the expectant underwater superoleophobicity characteristics, which were investigated by the test of WCA and UOCA. In air, the WCA and the pure water permeation flux of the substrate,

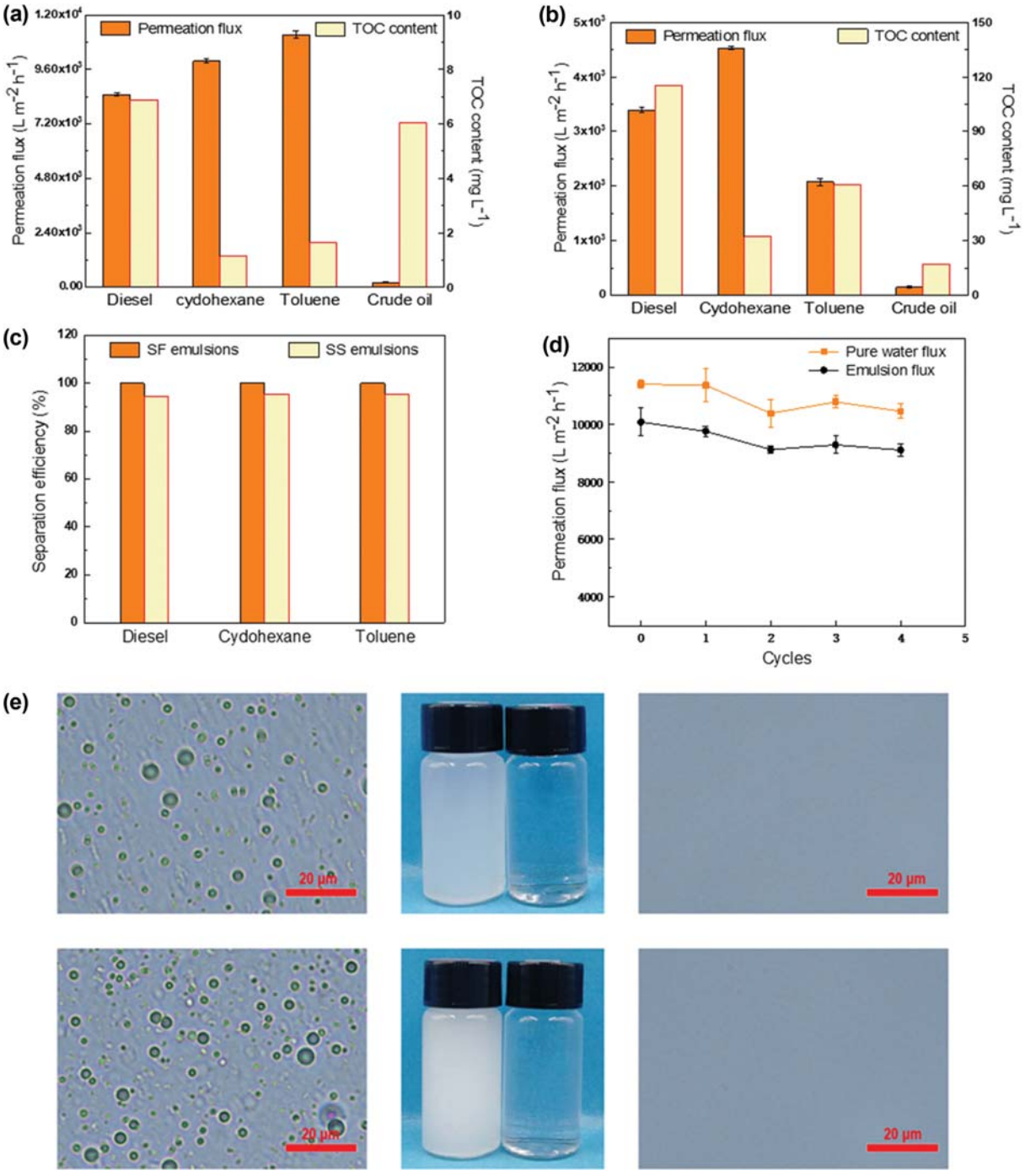

Fig. 4. (a), (b) The permeation flux and TOC content of CNF@PDA membrane for different SF and SS emulsions, respectively. (c) The separation efficiency of CNF@PDA membrane for various SF and SS emulsions, respectively. (d) Recyclability test for five cycles on the CNF@PDA membrane. (e) Optical microscopic photographs of feed and filtrated solutions.

PDA-coated membrane and CNF@PDA membrane are ~67°, 32° and 24°, ~13,924, 12,196, 11,320 L m^{-2} h^{-1}, respectively. As indicated in Fig. 2(a), the WCA of membrane decreased from 67° to 24° and the WCA of pure CNF membrane was 25.7° (Fig. S3, supporting information) revealing that the CNF modified on the PDA-coated membrane successfully. Besides, pure water permeation flux of CNF@PDA membrane also decreased from 13,329 to 11,320 L m^{-2} h^{-1}, which could be attributed to diminution of porosity and pore radius. Moreover, for CNF@PDA membrane, UOCA of 157.3° for dichloromethane, 154.1° for diesel, 154.1° for cyclohexane, 156.6° for toluene, 150.3° for crude oil, respectively, confirming its underwater superoleophobicity in Fig. 2(b). In contrast, the UOCA of dichloromethane on substrates and PDA-coated membranes was lower with 133.5° and 150.1°, respectively, suggesting that the CNF reaction on the membrane could improve its underwater superoleophobicity (Fig. S3, Supporting Information). We should emphasize that the substrate and PDA-coated membrane were easily adhered by crude oil with UOCAs from 25.0° to 140° and the pure CNF membrane was too dense with extremely low water flux, which could not fit for complicated oil/water separation. Besides, the underwater oil adhesion measurement on PDA-coated membrane and CNF@PDA membrane was carried out (Fig. 3(a), (b)). After compressing dichloromethane droplets on the underwater modified membranes, dichloromethane droplets were compressed to from a spherical to an ellipsoidal shape. After dichloromethane droplets were removed, oil droplets displayed obvious deformation on the PDA-coated membrane but no obvious deformation or adhesion on CNF@PDA membrane. Due to great underwater anti-oil-adhesion capability, the CNF@PDA membrane exhibited prominent underwater antifouling property to various oils. To further demonstrate the underwater low adhesion of membranes, crude oil fouled pre-wet membranes were soaked in water and crude oil completely adhering on the PDA-coated membrane in this time (Fig. 3(c); Movie S4, Supporting Information). On the contrary, the oil detached from the CNF@PDA membrane rapidly after immersing into water (Fig. 3(d); Movie S5, Supporting Information), indicating excellent antifouling performance of the CNF@PDA membrane. The antifouling mechanism is shown in Fig. 3(e), the anti-oil-adhesion property was contributed by the good water adsorption capacity of the CNF@PDA membrane, in which the absorbed water could develop a strong hydrated layer to restrain direct contact of oil with the membrane. Above results validated that CNF@PDA membranes were underwater superoleophobic with extremely low underwater oil adhesiveness and would be potential materials for oily wastewater separation.

3. Membrane Performance for Separating Oil-in-water Emulsions

Various oil/water emulsions were designed to assess oil/water emulsion separation performance of CNF@PDA membrane. As illustrated in Fig. 4(a), (b), the corresponding permeation fluxes of SF emulsions obtained from diesel, cyclohexane, toluene and crude oil were 8,488.96, 9,676.47, 11,126.99 and 203.73 L m^{-2} h^{-1}, respectively. The variation of permeation flux may be due to the differences from both the viscosity and oil droplet concentration of the

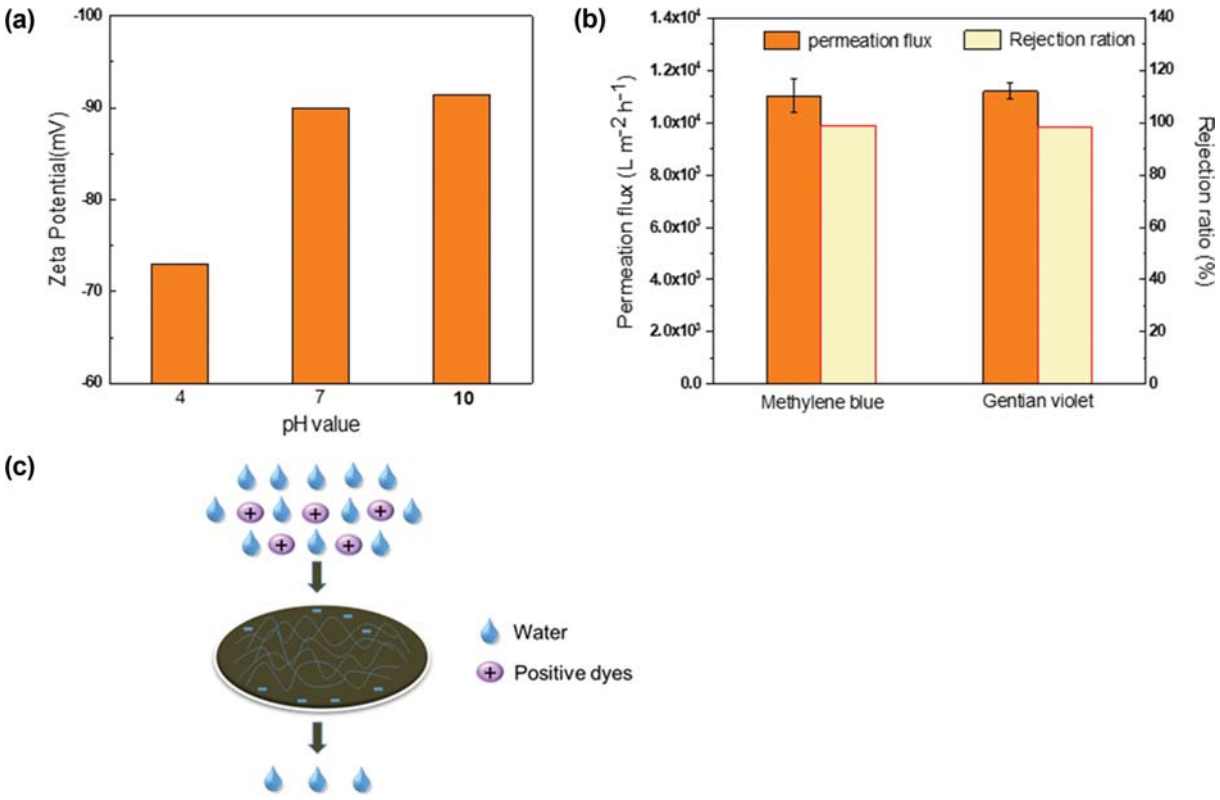

Fig. 5. (a) Zeta potential of CNF@PDA membrane under diverse pH conditions. (b) Permeation flux and rejection ratio of CNF@PDA for MB and GV dye solutions, respectively. (c) Mechanism of CNF@PDA membrane for removing oil and positive dyes, respectively.

emulsion which are formed by different types of oil. For other SS emulsions, the permeation fluxes of diesel, cyclohexane, toluene and crude oil were 3,395.59, 4,525.44, 2,073.01 and 149.41 L m^{-2} h^{-1}, respectively, which were relatively lower than SF emulsions due to the intervention of the surfactant. The oil concentration in the filtrates and emulsions was calculated by a TOC analyzer and corresponding separation efficiencies are shown in Fig. 4(c). As for SF emulsions involving diesel, cyclohexane and toluene, the separation efficiencies were 99.91%, 99.98% and 99.97%, respectively. While for SS emulsions, the separation efficiencies were 98.55%, 99.51% and 99.23%, respectively. Above results showed that the CNF@PDA membrane had great permeation fluxes and separation efficiencies.

The digital photographs and optical microscopic photographs of the feed and filtrated solutions of the diesel based SF emulsions and SS emulsions are shown in Fig. 4(e). Both the initial SF and SS emulsions were milky with numerous micrometer and sub-micrometer oil droplets. After filtration, the filtrate was clear and colorless and no oil droplet could be seen in photographs, which demonstrated the CNF@PDA membrane hold a good separation efficiency.

Generally, membranes always encounter oil-fouling problems, which seriously limit their actual application. Therefore, the ability of CNF@PDA membranes FRR was estimated. As indicated in Fig. 4(d), after five times of cycle, FRR of the substrate was very slow, almost could be negligible and the CNF@PDA membrane was 91.7%. This result demonstrated that the CNF@PDA membrane processed the good recovery performance and exhibited excellent antifouling property.

4. Membrane Performance for Separating Dye Solutions

Fig. 5(a) is zeta potential of CNF@PDA membrane under different pH conditions. The zeta potential was always negative from the pH of 4 to 10, which indicated the membrane surface was negatively charged. Due to electrostatic attraction, it helped us to separate positive dyes. The dye rejection performance of CNF@PDA membrane, a series of methylene blue (MB) and gentian violet (GV) dye solution were prepared with feed concentration of 5 mg L^{-1}. Fig. 5(b) shows the rejection rate of the charged dyes and the dye permeation fluxes of CNF@PDA membrane, MB and GV, were 99.07%, 98.02% and ~11,038, 11,215 L m^{-2} h^{-1}, respectively. Fig. S5(a), (b) (Supporting Information) illustrated changes in the absorbance spectra of the feed and filtrated dye solutions. The illustrations in Fig. S5(a), (b) (Supporting Information) show color changes of the feed and performance of CNF@PDA membrane for MB and GV. As described in Fig. 5(c), the dye molecules were retained by absorption of functional groups and electrostatic interaction, which contributed to a high separation speed and high removal rate of MB and GV.

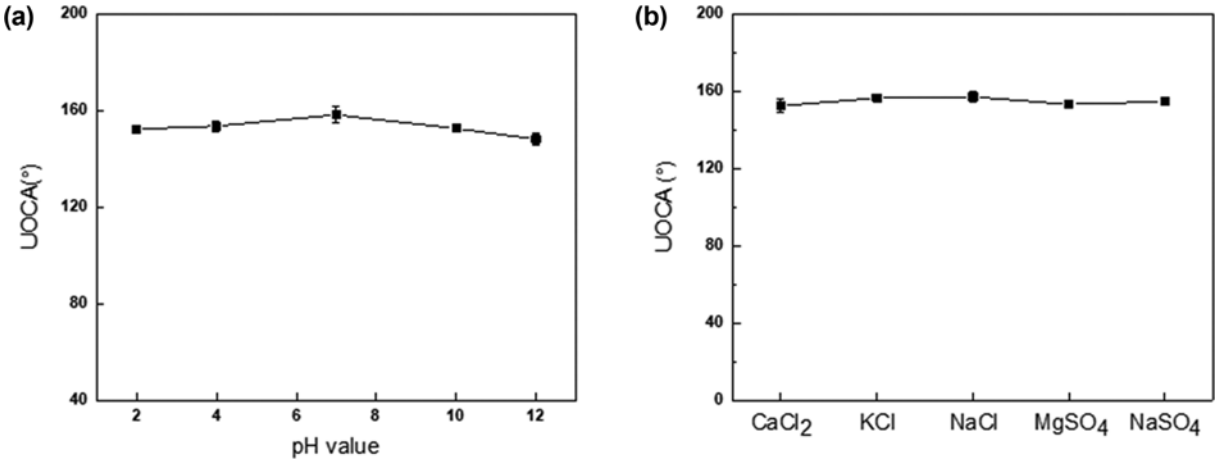

Fig. 6. (a) UOCA of CNF@PDA after the exposure to in different water with pH from 2 to 12 for 120 h. (b) UOCA of CNF@PDA after being kept in various 50 mg ml^{-1} salt solutions for 120 h.

Table 3. Literature review of other separation membranes

Materials	Application	Oil/water flux (L m^{-2} h^{-1})	Crude oil/water flux (L m^{-2} h^{-1})	Rejection	Sources
DA/KH550/TiO_2	Oil/water emulsion separation	382-605	-	>98%	[54]
GO/DA/HNTs	Dyes, heavy metal rejection and oil/water emulsion separation	23.53-60.32	-	~99%	[55]
PVDF/DA/tetraethoxysilane	Oil/water emulsion separation	140 (gravity)	-	-	[56]
DA/polyethyleneimine	Oil/water emulsion separation	100	-	~98%	[57]
Tunicate cellulose nanocrystal/palygorskite nanorod	Oil/water emulsion separation	1036-1734	-	>99%	[43]
Nanocellulose/DA	Oil/water emulsion separation and dye rejection	2073-4525	149	>98%	This work

5. Stability of CNF@PDA Membrane

For practical oily water treatment, the stability of membrane performance is an important and difficult issue. The stability of CNF@PDA membrane was conducted under rigorous conditions. The CNF@PDA membrane also maintained underwater superoleophobicity after the exposure to in different water with pH from 2 to 12 for 120 h and different salt solution for 120 h, including 50 mg ml^{-1} $CaCl_2$, KCl, NaCl, $MgSO_4$, $NaSO_4$ solutions. As shown in Fig. 6(a), (b), the UOCA values were 148.2-158.3°, 152.6-157.2° for different pH values and salty solutions, respectively. These results indicated that the stable surface wettability of CNF@PDA membrane in these corrosive liquids.

6. Compared with other Literature

Table 3 presents a literature review of other reported oil/water separation membranes. Compared with other separation membranes, the CNF@PDA membrane holds excellent oil/water separation efficiency and dye rejection efficiency. In addition, it can separate crude oil/water emulsion with good antifouling properties. Therefore, the modified composite membrane has a prospective application.

CONCLUSION

A polyelectrolyte CNF@PDA membrane was fabricated by a facile method and the membrane was equipped with excellent underwater superoleophobic property, high permeation flux and separation efficiency for emulsion separation and excellent antifouling property. Because of the functional layer of CNF, the membrane not only can separate both SF and SS oil/water emulsions but also can separate positive dyes with high permeation fluxes and rejection ratio. This method is expected to be used in designing and preparing the next generation of specific membranes for oil/water emulsions separation.

ACKNOWLEDGEMENTS

We are very grateful to the National Natural Science Foundation of China (51774245), Applied Basic Research Program of Science and Technology Department of Sichuan Province (No. 2018JY0517) for their financial support for this study.

CONFLICT OF INTEREST

We have no conflict of interest to declare.

SUPPORTING INFORMATION

Additional information as noted in the text. This information is available via the Internet at http://www.springer.com/chemistry/journal/11814.

REFERENCES

1. Z. Zhu, W. Wang and D. Qi, *Adv. Mater.*, **30**, 1801870 (2018).
2. A. K. Kota, G. Kwon, W. Choi, J. M. Mabry and A. Tuteja, *Nat. Commun.*, **3**, 1025 (2012).
3. S. Jo and Y. Kim, *Korean J. Chem. Eng.*, **33**, 3203 (2016).
4. G. Jiang, J. Li and Y Nie, *Environ. Sci. Technol.*, **50**, 7650, (2016).
5. W. Wallau, C. Schlawitschek and H. Arellano-Garcia, *Ind. Eng. Chem. Res.*, **55**, 4585 (2016).
6. Y. Lu and W. Yuan, *ACS Appl. Mater. Interfaces*, **9**, 29167 (2017).
7. X. Chen, L. Liu, K. Liu, Q. Miao and Y. Fang, *J. Mater. Chem. A*, **2**, 10081 (2014).
8. B. Das, B. Chakrabarty and P. Barkakati, *Korean J. Chem. Eng.*, **34**, 2559 (2017).
9. X. Chen, L. Liu, K. Liu, Q. Miao and Y. Fang, *J. Mater. Chem. A*, **2**, 10081 (2014).
10. L. Shao, X. Cheng, Z. Wang, J. Ma and Z. Guo, *J. Membr. Sci.*, **452**, 82 (2014).
11. H.-C. Yang, J. Luo, Y. Lv, P. Shen and Z.-K. Xu, *J. Membr. Sci.*, **483**, 42 (2015).
12. G.-d. Kang and Y.-m. Cao, *J. Membr. Sci.*, **463**, 145 (2014).
13. J. Ma, Y. He, H. Shi, Y. Fan, H. Yu and Y. Li, *J. Mater. Sci.*, **54**, 2241 (2019).
14. L. Zhang, Y. He and L. Ma, *ACS Appl. Mater. Interfaces*, **11**, 34487 (2019).
15. X. Zhao, Y. Su and J. Cao, *J. Mater. Chem. A*, **3**, 7287 (2015).
16. W. Zhang, Y. Zhu and X. Liu, *Angew. Chem., Int. Ed.*, **53**, 856 (2014).
17. S. Kasemset, A. Lee, D. J. Miller, B. D. Freeman and M. M. Sharma, *J. Membr. Sci.*, **425**, 208 (2013).
18. D.-G. Kim, H. Kang, S. Han and J.-C. Lee, *ACS Appl. Mater. Interfaces*, **4**, 5898 (2012).
19. N. Hilal, O. O. Ogunbiyi, N. J. Miles and R. Nigmatullin, *Sep. Sci. Technol.*, **40**, 1957 (2005).
20. Y.-F. Zhao, L.-P. Zhu, Z. Yi, B.-K. Zhu and Y.-Y. Xu, *J. Membr. Sci.*, **440**, 40 (2013).
21. T. Wang, Y. Wang and Y. Su, *Colloids Surf., B*, **46**, 233 (2005).
22. Y. Wang, Y. He, S. Yan, X. Yin and J. Chen, *Colloids Surf., A*, **582**, 123891 (2019).
23. J. Shin, H. Kim and H. Moon, *Korean J. Chem. Eng.*, **35**, 1319 (2018).
24. M. Amirilargani, M. Sadrzadeh, E. Sudhölter and L. de Smet, *Chem. Eng. J.*, **289**, 562 (2016).
25. A. Zaibudeen and J. Philip, *Colloids Surf., A*, **550**, 209 (2018).
26. B. Yin and C. Liu, *J. Nanosci. Nanotechnol.*, **19**, 3647 (2019).
27. P. S. Brown and B. Bhushan, *Sci. Rep.*, **5**, 8701 (2015).
28. F. Zhang, S. Gao, Y. Zhu and J. Jin, *J. Membr. Sci.*, **513**, 67 (2016).
29. K. He, H. Duan, G. Y. Chen, X. Liu, W. Yang and D. Wang, *ACS Nano*, **9**, 9188 (2015).
30. Y. Zhu, F. Zhang, D. Wang, X. F. Pei, W. Zhang and J. Jin, *J. Mater. Chem. A*, **1**, 5758 (2013).
31. Y.-H. Chiao, S.-T. Chen and T. Patra, *Desalination*, **469**, 114090 (2019).
32. J. P. F. Lagerwall, C. Schütz and M. Salajkova, *NPG Asia Mater.*, **6**, e80 (2014).
33. M. Jonoobi, R. Oladi and Y. Davoudpour, *Cellulose*, **22**, 935 (2015).
34. A. Dufresne, *Mater. Today*, **16**, 220 (2013).
35. K.-Y. Lee and Y. Aitomäki, *Compos. Sci. Technol.*, **105**, 15 (2014).
36. D. Klemm, F. Kramer and S. Moritz, *Angew. Chem., Int. Ed.*, **50**, 5438 (2011).
37. M. Smyth, M.-S. M'bengue, M. Terrien, C. Picart, J. Bras and E. J. Foster, *Carbohydr. Polym.*, **179**, 186 (2018).

38. T. Liu, Q.-F. An, X.-S. Wang, Q. Zhao, B.-K. Zhu and C.-J. Gao, *Carbohydr. Polym.*, **106**, 403 (2014).
39. J.-S. Yeo, O. Y. Kim and S.-H. Hwang, *J. Ind. Eng. Chem.*, **45**, 301 (2017).
40. B. S. Lalia, E. Guillen, H. A. Arafat and R. Hashaikeh, *Desalination*, **332**, 134 (2014).
41. Z. Jiang, Y. Fang and J. Xiang, *J. Phys. Chem. B*, **118**, 10250 (2014).
42. A. Dufresne, *Nanocellulose: from nature to high performance tailored materials*, Walter de Gruyter, Berlin (2012).
43. H. Zhan, T. Zuo, R. Tao and C. Chang, *ACS Sustainable Chem. Eng.*, **6**, 10833 (2018).
44. J. Jiang, L. Zhu, L. Zhu, H. Zhang, B. Zhu and Y. Xu, *ACS Appl. Mater. Interfaces*, **5**, 12895 (2013).
45. A. Postma, Y. Yan, Y. Wang, A. N. Zelikin, E. Tjipto and F. Caruso, *Chem. Mater.*, **21**, 3042 (2009).
46. Q. Liu, N. Wang, J. Caro and A. Huang, *J. Am. Chem. Soc.*, **135**, 17679 (2013).
47. H. Lee, S. M. Dellatore, W. M. Miller and P. B. Messersmith, *Science*, **318**, 426 (2007).
48. Y. Liu, K. Ai and L. Lu, *Chem. Rev.*, **114**, 5057 (2014).
49. Y. Liao, Y. Wang, X. Feng, W. Wang, F. Xu and L. Zhang, *Mater. Chem. Phys.*, **121**, 534 (2010).
50. P. Patchiya and R. Prasert, *Carbon Resources Conversion*, **1**, 32 (2018).
51. N. Lin, C. Bruzzese and A. Dufresne, *ACS Appl. Mater. Interfaces*, **4**, 4948 (2012).
52. A. R. D. O. Junior, M. M. F. Ferrarezi, I. V. P. Yoshida and M. D. C. Gonçalves, *J. Appl. Polym. Sci.*, **123**, 2027 (2011).
53. A. D. Dwivedi, N. D. Sanandiya and J. P. Singh, *ACS Sustainable Chem. Eng.*, **5**, 518 (2016).
54. H. Shi, Y. He and Y. Pan, *J. Membr. Sci.*, **506**, 60 (2016).
55. Q. Cheng, D. Ye, C. Chang and L. Zhang, *J. Membr. Sci.*, **525**, 1 (2017).
56. Z. Wang, X. Jiang, X. Cheng, C. H. Lau and L. Shao, *ACS Appl. Mater. Interfaces*, **7**, 9534 (2015).
57. H.-C. Yang, K.-J. Liao, H. Huang, Q.-Y. Wu, L.-S. Wan and Z.-K. Xu, *J. Mater. Chem. A*, **2**, 10225 (2014).

Supporting Information

Bio-inspired antifouling Cellulose nanofiber multifunctional filtration membrane for highly efficient emulsion separation and application in water purification

Xiangying Yin[*,], Yi He[*,**,†], Yuqi Wang[*,**], Hao Yu[*,**], Jingyu Chen[***,†], and Yixuan Gao[*,**]**

*State Key Laboratory of Oil & Gas Reservoir Geology and Exploitation, Southwest Petroleum University, Chengdu, Sichuan 610500, P. R. China
**College of Chemistry and Chemical Engineering, Southwest Petroleum University, Chengdu, Sichuan 610500, P. R. China
***Deakin University, Institute for Frontier Materials, VIC 3220, Australia
(*Received 19 June 2019 • Revised 25 March 2020 • Accepted 5 May 2020*)

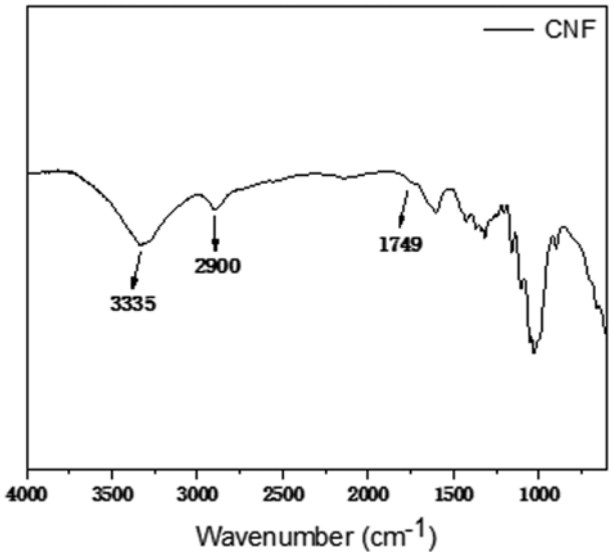

Fig. S1. FT-IR of pure CNF membrane.

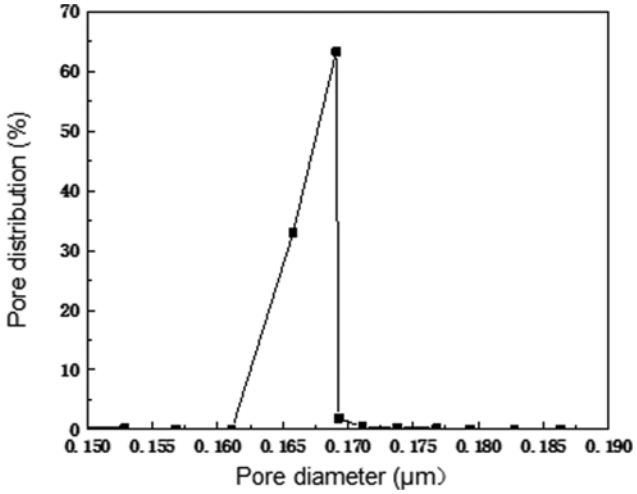

Fig. S2. The pore diameter and pore distribution of PDA@CNF membrane are determined by bubble pressure membrane pore size analyzer.

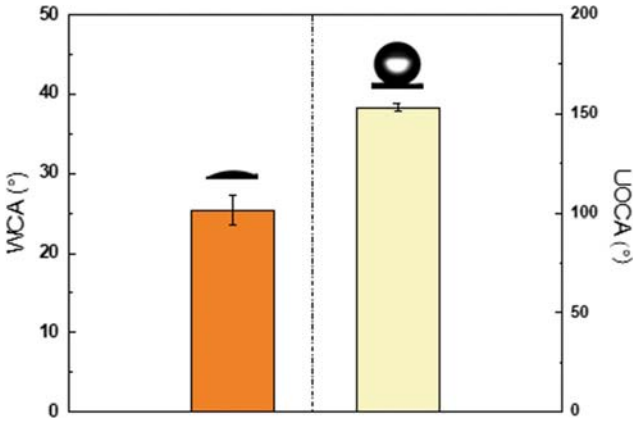

Fig. S3. The WCA and UOCA of pure CNF membrane.

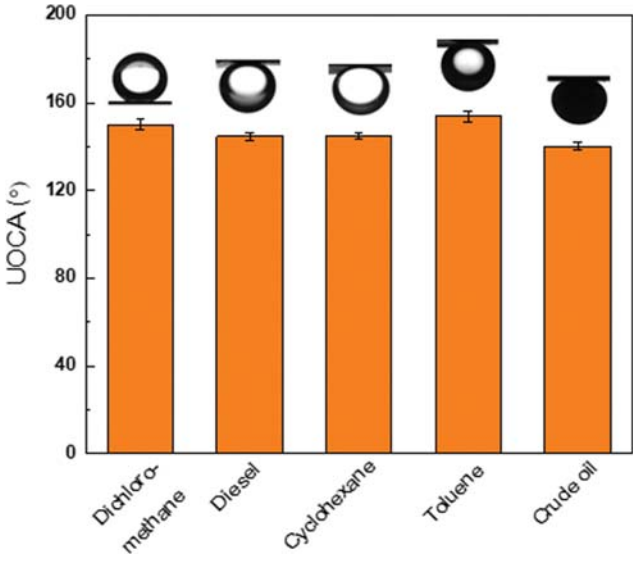

Fig. S4. UOCA for various oils of PDA-coated membranes.

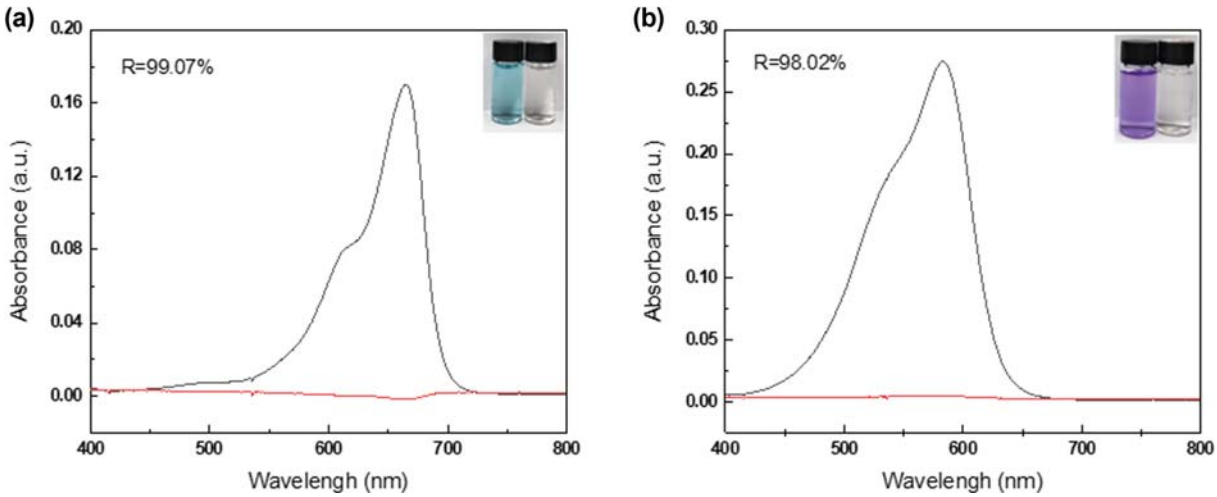

Fig. S5. (a), (b) The UV-vis spectral changes before and after filtering for MB and GV dye solutions.